Constraining new physics from Higgs measurements with Lilith: update to LHC Run 2 results

Thi Nhung Dao[1], Sabine Kraml[2*], Duc Ninh Le[1], Loc Tran Quang[1]

1 Institute For Interdisciplinary Research in Science and Education, ICISE, 590000, Quy Nhon, Vietnam
2 Laboratoire de Physique Subatomique et de Cosmologie, Université Grenoble-Alpes, CNRS/IN2P3, 53 Avenue des Martyrs, F-38026 Grenoble, France
* sabine.kraml@lpsc.in2p3.fr

June 6, 2019

Abstract

Lilith is public python library for constraining new physics from Higgs signal strength measurements. We here present version 2.0 of Lilith together with an updated database which includes the full set of ATLAS and CMS Run 2 Higgs results for 36 fb^{-1}. Both the code and the XML database where extended from the ordinary Gaussian approximation employed in Lilith-1.1 to using variable Gaussian and Poisson distributions. Moreover, Lilith can now make use of correlation matrices of arbitrary dimension. We provide detailed validations of the implemented experimental results as well as a status of global fits for *i)* reduced Higgs couplings and *ii)* Two-Higgs-doublet models of Type-I and Type-II. Lilith-2.0 is available on GitHub and ready to be used to constrain a wide class of new physics scenarios.

1 Introduction

Introduce Higgs couplings fits and `Lilith` [1] .....
.....
.....
.....
.....
.....
.....

2 Extended XML format for experimental input

In the `Lilith` database, every single experimental result is stored in a separate XML file. This allows to easily select the results to use in a fit, and it also makes maintaining and updating the database rather easy.

The root tag of each XML file is `<expmu>`, which has two mandatory attributes, `dim` and `type` to specify the type of signal strength result. Production and decay modes are specified via `prod` and `decay` attributes either directly in the `<expmu>` tag or as efficiencies in `<eff>` tags. Additional (optional) information can be provided in `<experiment>`, `<source>`, `<sqrts>`, `<CL>` and `<mass>` tags. Taking the $H \to \gamma\gamma$ result from the combined ATLAS and CMS Run 1 analysis [2] as a concrete example, the structure of the XML file is

```
<expmu decay="gammagamma" dim="2" type="n">
  <experiment>ATLAS-CMS</experiment>
  <source type="publication">CMS-HIG-15-002; ATLAS-HIGG-2015-07</source>
  <sqrts>7+8</sqrts>
  <mass>125.09</mass>
  <CL>68%</CL>

  <eff axis="x" prod="ggH">1.</eff>
  <eff axis="y" prod="VVH">1.</eff>

  <!-- (...) -->
</expmu>
```

where `<!-- (...) -->` is a placeholder for the actual likelihood information. For a detailed description, we refer to the original `Lilith` manual [1]. In the following, we assume that the reader is familiar with the basic syntax.

So far, the likelihood information could be specified in one or two dimensions in the form of [1]: 1D intervals given as best fit with 1σ error; 2D likelihood contours described as best fit point and parameters a, b, c which parametrize the inverse of the covariance matrix; or full likelihood information as 1D or 2D grids of $-2\log L$. The first two options, 1D intervals and 2D likelihood contours, declared as `type="n"` in the `<expmu>` tag, employ an ordinary Gaussian approximation; in the 1D case, asymmetric errors are accounted for by putting together two one-sided Gaussians with the same mean but different variances, while the 2D case assumes symmetric errors. This does does not always allow to describe the experimental data (i.e. the true likelihood) very well. Full 2D likelihood grids would be much better but are rarely available.

In order to treat asymmetric uncertainties in a better way, we have extended the XML format and fitting procedure in `Lilith` to Gaussian distributions of variable width ("variable Gaussian") as well as generalized Poisson distributions. The declaration is `type="vn"` for variable Gaussian or `type="p"` for Poisson distribution in the `<expmu>` tag. Both work for 1D and 2D data with the same syntax. Moreover, in order to make use of the N-dimensional ($N > 2$) correlation matrices which both ATLAS and CMS have started to provide, we have added a new XML format for correlated signal strengths in more than two dimensions. This can be used with the ordinary or variable Gaussian approximation for the likelihood. In the following we give explicit examples for the different possibilities.

1D likelihood parameterization

For 1D data, the format remains the same as in [1]. For example, a signal strength $\mu(ZH,\, b\bar{b}) = 1.12^{+0.50}_{-0.45}$ is implemented as

```
<bestfit>1.12</bestfit>
<param>
  <uncertainty side="left">-0.45</uncertainty>
  <uncertainty side="right">0.50</uncertainty>
</param>
```

The `<bestfit>` tag contains the best-fit value, while the `<uncertainty>` tag contains the left (negative) and right (positive) 1σ errors.[1] The choice of likelihood function is done by setting `type="n"` for ordinary, 2-sided Gaussian (as in `Lilith-1.1`); `type="vn"` for a variable Gaussian; or `type="p"` for a Poisson distribution in the `<expmu>` tag.

2D likelihood parameterization

For `type="vn"` and `type="p"`, signal strengths in 2D with a correlation are now described in an analogous way as 1D data. For example, $\mu(\mathrm{ggH}, WW) = 1.10^{+0.21}_{-0.20}$ and $\mu(\mathrm{VBF}, WW) = 0.62^{+0.36}_{-0.35}$ with a correlation of $\rho = -0.08$ can be implemented as

```
<expmu decay="WW" dim="2" type="vn">

  <eff axis="x" prod="ggH">1.0</eff>
  <eff axis="y" prod="VBF">1.0</eff>

  <bestfit>
    <x>1.10</x>
    <y>0.62</y>
  </bestfit>

  <param>
    <uncertainty axis="x" side="left">-0.20</uncertainty>
    <uncertainty axis="x" side="right">+0.21</uncertainty>
    <uncertainty axis="y" side="left">-0.35</uncertainty>
    <uncertainty axis="y" side="right">+0.36</uncertainty>
    <correlation>-0.08</correlation>
  </param>
</expmu>
```

Here, the `<eff>` tag is used to declare the `x` and `y` axes. The `<bestfit>` tag specifies the location of the best-fit point in the (`x`,`y`) plane. The `<uncertainty>` tags contain the left (negative) and right (positive) 1σ errors for the `x` and `y` axes, and finally the `<correlation>` tag specifies the correlation between `x` and `y`. The choice of likelihood function is again done by setting `type="vn"` or `type="p"` in the `<expmu>` tag.

To ensure backwards compatibility, `type="n"` however still requires the tags `<a>`, `<b>`, `<c>` to give the inverse of the covariance matrix instead of `<uncertainty>` and `<correlation>`, see [1].

[1] The values in the `<uncertainty>` tag can be given with or without a sign.

Multi-dimensional data

For correlated signal strengths in more than 2 dimensions, a new format is introduced. We here illustrate it by means of the CMS result [3], which has signal strengths for 24 production and decay mode combinations plus a 24×24 correlation matrix. First, we set `dim="24"` and label the various signal strengths as axes d1, d2, d3, ... d24:[2]

```
<expmu dim="24" type="vn">
  <eff axis="d1" prod="ggH" decay="gammagamma">1.0</eff>
  <eff axis="d2" prod="ggH" decay="ZZ">1.0</eff>
  <eff axis="d3" prod="ggH" decay="WW">1.0</eff>
  ...
  <eff axis="d24" prod="ttH" decay="tautau">1.0</eff>
```

The best-fit values for each axis are specified as

```
  <bestfit>
    <d1>1.16</d1>
    <d2>1.22</d2>
    <d3>1.35</d3>
    ...
    <d24>0.23</d24>
  </bestfit>
```

The `<param>` tag then contains the uncertainties and correlations in the form

```
  <param>
    <uncertainty axis="d1" side="left">-0.18</uncertainty>
    <uncertainty axis="d1" side="right">+0.21</uncertainty>
    <uncertainty axis="d2" side="left">-0.21</uncertainty>
    <uncertainty axis="d2" side="right">+0.23</uncertainty>
    ...
    <uncertainty axis="d24" side="left">-0.88</uncertainty>
    <uncertainty axis="d24" side="right">+1.03</uncertainty>

    <correlation entry="d1d2">0.12</correlation>
    <correlation entry="d1d3">0.16</correlation>
    <correlation entry="d1d4">0.08</correlation>
    ...
    <correlation entry="d23d24">0</correlation>
  </param>
</expmu>
```

This will also work for `type="n"`.

[2] The `<experiment>`, `<source>`, `<sqrts>`, etc. tags are omitted for brevity.

3 Likelihood calculation

For the variable Gaussian, the computation of the likelihood in `computelikelihood.py` follows Section 3.6 “Variable Gaussian (2)” of [4]. The Poisson distribution is implemented according to Section 3.4 “Generalised Poisson”, eq. (10a), of [4].

..... give explicit equations and explain implementation i the code ....

4 ATLAS and CMS results included in the database update

4.1 ATLAS Run 2 results for 36 fb^{-1}

The ATLAS Run 2 results included in this release are summarised in Table 1 and explained in more detail below.

mode	$\gamma\gamma$	ZZ^*	WW^*	$\tau\tau$	$b\bar{b}$	inv.
ggH	[5]	[6]	[7]	[8]	–	–
VBF	[5]	[6]	[7]	[8]	[9]	–
WH	[5]	[6]	–	–	[10]	–
ZH			–	–	[10]	[11]
ttH	[5, 12]	[6, 12]	[12]	[12]	[12, 13]	–

Table 1: Overview of ATLAS Run 2 results included in this release.

***H* → γγ (HIGG-2016-21):** The ATLAS analysis [5] provides in Fig. 12 $H \to \gamma\gamma$ signal strengths separated into ggH, VBF, VH and "top" (ttH+tH) production modes. Since no correlations are given for the signal strengths, we use instead the correlations for the stage-0 simplified template cross sections (STXS) provided in Fig. 40a of the ATLAS paper, which should be a close enough match. It turns out that these data do not allow to reproduce very well the ATLAS coupling fits for $(C_V,\ C_F)$ or $(C_\gamma,\ C_g)$. The reason seems to be that the μ values rounded to one decimal are not precise enough. We have therefore extracted the best-fit points and uncertainties from fits to the 1D profile likelihoods, which are provided as Auxiliary Figures 23a–d on the analysis webpage. and used these together with the STXS correlations in the `Lilith` XML file. This gives a better coupling fit, as shown in the validation plots in Fig. 1.

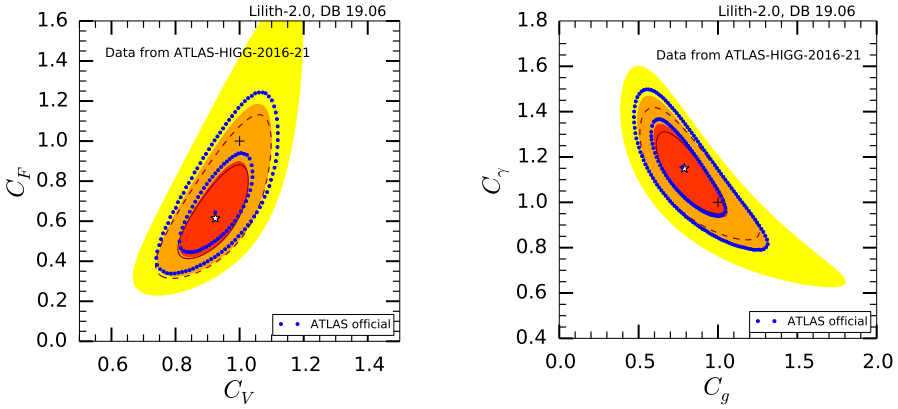

Figure 1: Fit of C_F vs. C_V (left) and C_γ vs. C_g (right) for data from the ATLAS $H \to \gamma\gamma$ analysis [3]. The red, orange and yellow filled areas show the 68%, 95% and 99.7% CL regions obtained with `Lilith` using best-fit values and uncertainties for the signal strengths as extracted from Aux. Figs. 23a–d of the ATLAS analysis together with the correlation matrix for the stage-0 STXS. This can be compared to the 68%, 95% CL contours obtained using the rounded values from Fig. 12 of [3] (solid and dashed dark red lines) and to the official 68%, 95% CL contours from ATLAS (blue dots).

We note that the same fit quality is obtained when using only the correlation between ggH and VBF production modes (as 2D data) and treating VH and ttH as independent (as 1D data). The relevant XML files are all included in the database, so the user can choose

the preferred combination. This is relevant to avoid double counting when combining this with other measurements, concretely with the data from [12].

***$H \to ZZ^* \to 4l$* (HIGG-2016-22):** A similar issue as discussed for $H \to \gamma\gamma$ above arises when using the signal strengths given in Table 9 of [6] together with the correlation matrix given in Aux. Fig. 4a. We therefore use μ(ggH, ZZ^*) and μ(VBF, ZZ^*) extracted from the 1D profile likelihoods Aux. Figs. 7a and 7b with a correlation $\rho = -0.41$ according to Aux. Fig. 4c. For the VH and ttH production modes, we convert the given 95% CL limits into $\mu(\text{VH}, ZZ^*) = 0^{+1.85}_{-0.0}$ and $\mu(\text{ttH}, ZZ^*) = 0^{+3.75}_{-0.0}$. For validation, we compare to the C_F vs. C_V fit from ATLAS, see Fig. 2.

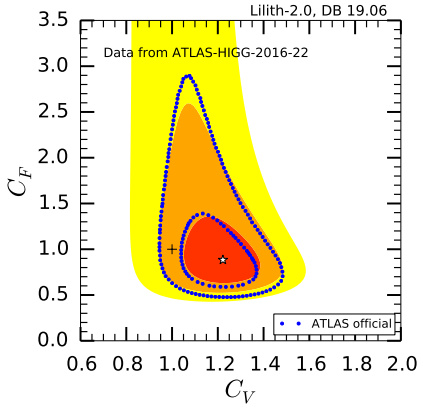

Figure 2: Fit of C_F vs. C_V for data from the ATLAS $H \to ZZ^*$ analysis [6]. The 68%, 95% and 99.7% CL regions obtained with `Lilith` are shown as red, orange and yellow areas, and compared to the 68%, 95% CL contours from ATLAS (in blue).

***$H \to WW^* \to 2l2\nu$* (HIGG-2016-07):**

***$H \to \tau\tau$* (HIGG-2017-07):**

***$H \to b\bar{b}$* (HIGG-2016-29 and HIGG-2016-30):**

***$H \to$* invisible (HIGG-2016-28):** Results from the search for invisibly decaying Higgs bosons produced in association with a Z boson are presented in [11]. Assuming the Standard Model ZH production cross-section, an observed (expected) upper limit of 67% (39%) at the 95% confidence level is set on BR($H \to inv$) for $m_H = 125$ GeV. We use $1 - \text{CLs}$ as function BR($H \to inv$) extracted from auxiliary Figure 1c on the analysis' webpage.

4.2 CMS Run 2 results for 36 fb^{-1}

The CMS Run 2 results included in this release are summarised in Table 2 and explained in more detail below.

mode	$\gamma\gamma$	ZZ^*	WW^*	$\tau\tau$	$b\bar{b}$	$\mu\mu$	inv.
ggH	[3]	[3]	[3]	[3]	[3]	[3]	[14]
VBF	[3]	[3]	[3]	[3]	–	[3]	[14]
WH	[3]	[3]	[3]	[15]	[3]	–	[14]
ZH	[3]	[3]	[3]	[15]	[3]	–	[14]
ttH	[3]	[3]	[3]	[3]	[3]	–	–

Table 2: Overview of CMS Run 2 results included in this release. Note that we use the full 24×24 correlation matrix for the signal strengths for each production and decay mode combination provided in [3].

Combined measurements (HIG-17-031): CMS presented in [3] a combination of the individual measurements for the $H \to \gamma\gamma$ [16], ZZ [17], WW [18], $\tau\tau$ [19], $b\bar{b}$ [20, 21] and $\mu\mu$ [22] decay modes as well as the $t\bar{t}H$ analyses [23–25]. We use the best fit values and uncertainties for the signal strengths for each production and decay mode combination presented in Table 3 of [3] together with the 24×24 correlation matrix provided as "Additional Figure 1" on the analysis webpage. As shown in Fig. 3, this allows to reproduce well the coupling fits of the CMS paper.

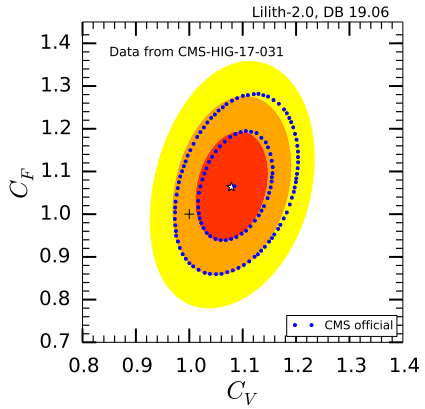

Figure 3: Fit of C_F vs. C_V using best-fit values and uncertainties for the signal strengths for each production (ggH, VBF, WH, ZH, ttH) and decay ($\gamma\gamma$, ZZ, WW, $\tau\tau$, $b\bar{b}$, $\mu\mu$) mode combination together with the 24×24 correlation matrix from the CMS combination paper [3]. The 1σ, 2σ and 3σ regions obtained with `Lilith` are shown as red, orange and yellow areas, and compared to the 1σ and 2σ contours from CMS (blue dots).

***VH*, $H \to \tau\tau$ (HIG-18-007)**: The above data from [3] is supplemented by the results for the $\tau\tau$ decay mode from the WH and ZH targeted analysis [15]. These are implemented in the form of 1D intervals for $\mu(ZH,\ H \to \tau\tau)$ and $\mu(WH,\ H \to \tau\tau)$ taken from Fig. 6 of [15].

***H* → invisible (HIG-17-023)**: In [14], CMS performed a search for invisible decays of a Higgs boson produced through vector boson fusion. We use the profile likelihood ratios for the qqH-tag, Z(ll)H-, V(qq')H- and ggH-tag categories extracted from their Fig. 8b

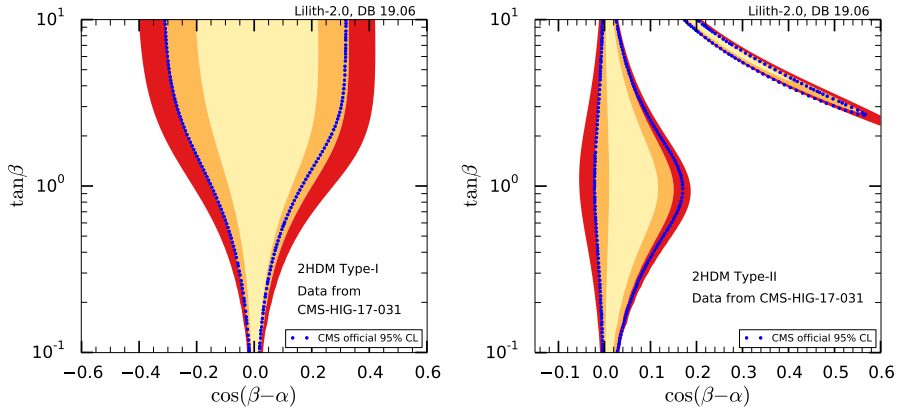

Figure 4: Fit of $\tan\beta$ vs. $\cos(\beta-\alpha)$ for the Two-Higgs-Doublet models of Type I (left) and Type II (right) using the data from the combined CMS measurement [3]. The beige, orange and red filled areas show the 68%, 95% and 99.7% CL regions obtained with `Lilith`, while the blue dots mark the 95% CL contours from CMS.

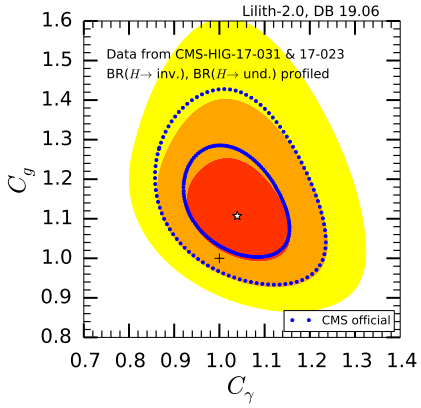

Figure 5: Fit of C_g vs. C_γ using the data from the combined CMS measurement [3] and the search for invisible decays of a Higgs boson [14]. The branching ratios of invisible and undetected decays are treated as free parameters in the fit. The 1σ, 2σ and 3σ regions obtained with `Lilith` are shown as red, orange and yellow areas, and compared to the 1σ and 2σ contours from CMS (in blue).

together with the relative contributions from the different Higgs production mechanisms given in Table 6 of that paper. This assumes that the relative signal contributions stay roughly the same as for SM production cross sections. For validation, we reproduce in Fig. 5 the C_g vs. C_γ fit of [3], where the branching ratios of invisible and undetected decays are treated as free parameters.[3]

[3] The profiling in Fig. 5 was done with `Minuit`. Since `Minuit` does not allow conditional limits, in this case $\mathrm{BR}(H \to \text{inv.}) + \mathrm{BR}(H \to \text{undetected}) < 1$, we demanded that both $\mathrm{BR}(H \to \text{inv.})$ and $\mathrm{BR}(H \to \text{undetected})$ be less than 50%.

5 Status of Higgs coupling fits

6 Conclusion

must include a conclusion.

Acknowledgements

S.K. thanks W. Adam, R. Schöfbeck, W. Waltenberger and N. Wardle for helpful discussions. This work was supported in part by the IN2P3 theory project "LHC-itools: methods and tools for the interpretation of the LHC Run 2 results for new physics". D.T.N. thanks the LPSC Grenoble for hospitality and financial support for a research visit within the LHC-itools project. L.T.Q. thanks the ICISE ...

A Overview of XML data files

B Implementation of 2D Poisson likelihood with correlation

References

[1] J. Bernon and B. Dumont, *Lilith: a tool for constraining new physics from Higgs measurements*, Eur. Phys. J. **C75**(9), 440 (2015), doi:10.1140/epjc/s10052-015-3645-9, 1502.04138.

[2] G. Aad *et al.*, *Measurements of the Higgs boson production and decay rates and constraints on its couplings from a combined ATLAS and CMS analysis of the LHC pp collision data at $\sqrt{s}$ = 7 and 8 TeV*, JHEP **08**, 045 (2016), doi:10.1007/JHEP08(2016)045, 1606.02266.

[3] A. M. Sirunyan *et al.*, *Combined measurements of Higgs boson couplings in proton–proton collisions at $\sqrt{s}$ = 13 TeV*, Eur. Phys. J. **C79**(5), 421 (2019), doi:10.1140/epjc/s10052-019-6909-y, https://cms-results.web.cern.ch/cms-results/public-results/publications/HIG-17-031/, 1809.10733.

[4] R. Barlow, *Asymmetric statistical errors*, In *Statistical Problems in Particle Physics, Astrophysics and Cosmology (PHYSTAT 05): Proceedings, Oxford, UK, September 12-15, 2005*, pp. 56–59 (2004), physics/0406120.

[5] M. Aaboud *et al.*, *Measurements of Higgs boson properties in the diphoton decay channel with 36 fb^{-1} of pp collision data at $\sqrt{s} = 13$ TeV with the ATLAS detector*, Phys. Rev. **D98**, 052005 (2018), doi:10.1103/PhysRevD.98.052005, https://atlas.web.cern.ch/Atlas/GROUPS/PHYSICS/PAPERS/HIGG-2016-21/, 1802.04146.

[6] M. Aaboud *et al.*, *Measurement of the Higgs boson coupling properties in the $H \to ZZ^* \to 4\ell$ decay channel at $\sqrt{s}$ = 13 TeV with the ATLAS detector*, JHEP **03**, 095 (2018), doi:10.1007/JHEP03(2018)095, https://atlas.web.cern.ch/Atlas/GROUPS/PHYSICS/PAPERS/HIGG-2016-22/, 1712.02304.

[7] M. Aaboud *et al.*, *Measurements of gluon-gluon fusion and vector-boson fusion Higgs boson production cross-sections in the $H \to WW^* \to e\nu\mu\nu$ decay channel*

in pp collisions at $\sqrt{s} = 13$ TeV with the ATLAS detector, Phys. Lett. **B789**, 508 (2019), doi:10.1016/j.physletb.2018.11.064, https://atlas.web.cern.ch/Atlas/GROUPS/PHYSICS/PAPERS/HIGG-2016-07, 1808.09054.

[8] M. Aaboud *et al.*, *Cross-section measurements of the Higgs boson decaying into a pair of τ-leptons in proton-proton collisions at $\sqrt{s} = 13$ TeV with the ATLAS detector*, Phys. Rev. **D99**, 072001 (2019), doi:10.1103/PhysRevD.99.072001, https://atlas.web.cern.ch/Atlas/GROUPS/PHYSICS/PAPERS/HIGG-2017-07, 1811.08856.

[9] M. Aaboud *et al.*, *Search for Higgs bosons produced via vector-boson fusion and decaying into bottom quark pairs in $\sqrt{s} = 13$ TeV pp collisions with the ATLAS detector*, Phys. Rev. **D98**(5), 052003 (2018), doi:10.1103/PhysRevD.98.052003, https://atlas.web.cern.ch/Atlas/GROUPS/PHYSICS/PAPERS/HIGG-2016-30, 1807.08639.

[10] M. Aaboud *et al.*, *Evidence for the $H \to b\bar{b}$ decay with the ATLAS detector*, JHEP **12**, 024 (2017), doi:10.1007/JHEP12(2017)024, https://atlas.web.cern.ch/Atlas/GROUPS/PHYSICS/PAPERS/HIGG-2016-29, 1708.03299.

[11] M. Aaboud *et al.*, *Search for an invisibly decaying Higgs boson or dark matter candidates produced in association with a Z boson in pp collisions at $\sqrt{s} = 13$ TeV with the ATLAS detector*, Phys. Lett. **B776**, 318 (2018), doi:10.1016/j.physletb.2017.11.049, https://atlas.web.cern.ch/Atlas/GROUPS/PHYSICS/PAPERS/HIGG-2016-28/, 1708.09624.

[12] M. Aaboud *et al.*, *Evidence for the associated production of the Higgs boson and a top quark pair with the ATLAS detector*, Phys. Rev. **D97**(7), 072003 (2018), doi:10.1103/PhysRevD.97.072003, https://atlas.web.cern.ch/Atlas/GROUPS/PHYSICS/PAPERS/HIGG-2017-02, 1712.08891.

[13] M. Aaboud *et al.*, *Search for the standard model Higgs boson produced in association with top quarks and decaying into a $b\bar{b}$ pair in pp collisions at $\sqrt{s} = 13$ TeV with the ATLAS detector*, Phys. Rev. **D97**(7), 072016 (2018), doi:10.1103/PhysRevD.97.072016, https://atlas.web.cern.ch/Atlas/GROUPS/PHYSICS/PAPERS/HIGG-2017-03, 1712.08895.

[14] A. M. Sirunyan *et al.*, *Search for invisible decays of a Higgs boson produced through vector boson fusion in proton-proton collisions at $\sqrt{s} = 13$ TeV* (2018), doi:10.1016/j.physletb.2019.04.025, https://cms-results.web.cern.ch/cms-results/public-results/publications/HIG-17-023/, 1809.05937.

[15] A. M. Sirunyan *et al.*, *Search for the associated production of the Higgs boson and a vector boson in proton-proton collisions at $\sqrt{s} = 13$ TeV via Higgs boson decays to τ leptons*, Submitted to: JHEP (2018), https://cms-results.web.cern.ch/cms-results/public-results/publications/HIG-18-007/, 1809.03590.

[16] A. M. Sirunyan *et al.*, *Measurements of Higgs boson properties in the diphoton decay channel in proton-proton collisions at $\sqrt{s} = 13$ TeV*, JHEP **11**, 185 (2018), doi:10.1007/JHEP11(2018)185, 1804.02716.

[17] A. M. Sirunyan *et al.*, *Measurements of properties of the Higgs boson decaying into the four-lepton final state in pp collisions at $\sqrt{s} = 13$ TeV*, JHEP **11**, 047 (2017), doi:10.1007/JHEP11(2017)047, 1706.09936.

[18] A. M. Sirunyan *et al.*, *Measurements of properties of the Higgs boson decaying to a W boson pair in pp collisions at* $\sqrt{s} = 13$ *TeV*, Phys. Lett. **B791**, 96 (2019), doi:10.1016/j.physletb.2018.12.073, 1806.05246.

[19] A. M. Sirunyan *et al.*, *Observation of the Higgs boson decay to a pair of* τ *leptons with the CMS detector*, Phys. Lett. **B779**, 283 (2018), doi:10.1016/j.physletb.2018.02.004, 1708.00373.

[20] A. M. Sirunyan *et al.*, *Evidence for the Higgs boson decay to a bottom quark–antiquark pair*, Phys. Lett. **B780**, 501 (2018), doi:10.1016/j.physletb.2018.02.050, 1709.07497.

[21] A. M. Sirunyan *et al.*, *Inclusive search for a highly boosted Higgs boson decaying to a bottom quark-antiquark pair*, Phys. Rev. Lett. **120**(7), 071802 (2018), doi:10.1103/PhysRevLett.120.071802, 1709.05543.

[22] A. M. Sirunyan *et al.*, *Search for the Higgs boson decaying to two muons in proton-proton collisions at* $\sqrt{s} = 13$ *TeV*, Phys. Rev. Lett. **122**(2), 021801 (2019), doi:10.1103/PhysRevLett.122.021801, 1807.06325.

[23] A. M. Sirunyan *et al.*, *Evidence for associated production of a Higgs boson with a top quark pair in final states with electrons, muons, and hadronically decaying* τ *leptons at* $\sqrt{s} = 13$ *TeV*, JHEP **08**, 066 (2018), doi:10.1007/JHEP08(2018)066, 1803.05485.

[24] A. M. Sirunyan *et al.*, *Search for* $\mathrm{t\bar{t}H}$ *production in the* $\mathrm{H} \to \mathrm{b\bar{b}}$ *decay channel with leptonic* $\mathrm{t\bar{t}}$ *decays in proton-proton collisions at* $\sqrt{s} = 13$ *TeV*, JHEP **03**, 026 (2019), doi:10.1007/JHEP03(2019)026, 1804.03682.

[25] A. M. Sirunyan *et al.*, *Search for* $\mathrm{t\bar{t}}H$ *production in the all-jet final state in proton-proton collisions at* $\sqrt{s} = 13$ *TeV*, JHEP **06**, 101 (2018), doi:10.1007/JHEP06(2018)101, 1803.06986.